Electronic Supporting information

for

Metal Substitution in a Lindqvist Polyoxometalate Leads to Improved Photocatalytic Performance

Johannes Tucher, Yanlin Wu, Leanne C. Nye, Ivana Ivanovic-Burmazovic, Marat M. Khusniyarov and Carsten Streb*
Department Chemistry and Pharmacy, Friedrich-Alexander-University Erlangen-Nuremberg, Egerlandstr. 1, 91058 Erlangen, Germany.
*Email: carsten.streb@chemie.uni-erlangen.de

1. Instrumentation

X-ray diffraction: Single-crystal X-ray diffraction studies were performed on a Nonius Kappa CCD Single-crystal X-ray diffractometer equipped with a graphite monochromator using MoKα radiation (wavelength $\lambda(\mathrm{MoK}_\alpha) = 0.71073$ Å).

NMR spectroscopy: ^{1}H- and ^{13}C-NMR spectroscopy was performed on a JEOL EX 270 NMR spectrometer or JEOL EX 400 spectrometer using deuterated solvents as internal standards.

UV-Vis spectroscopy: UV-Vis spectroscopy was performed on a Shimadzu UV-2401PC spectrophotometer or Varian Cary 50 spectrophotometer. All systems were used with standard cuvettes (d = 10.0 mm).

FT-IR spectroscopy: FT-IR spectroscopy was performed on a Shimadzu FT-IR-8400S spectrometer. Samples were prepared as KBR pellets. Signals are given as wavenumbers in cm^{-1} using the following abbreviations: vs = very strong, s = strong, m = medium, w = weak and b = broad.

Elemental analysis: Elemental analysis was performed on a Euro Vector Euro EA 3000 Elemental Analyzer.

Flame atomic absorption spectroscopy: Flame atomic absorption spectroscopy (FAAS) was performed on a Perkin Elmer 5100 PC Atomic Absorption System.

Electrospray ionization mass spectrometry: ESI-MS spectra were recorded on a Bruker Daltonics maXis ultra high resolution ESI-Time-Of-Flight MS. Spectra were obtained in negative-ion mode. Peaks were identified using simulated isotopic patterns created within the Bruker DataAnalysis software.

TD-DFT-Computations: Time-dependent density functional theory (TD-DFT) calculations were performed using ORCA ver. 2.7 rev. 0 (F. Neese, University of Bonn) using a B3LYP functional and TZVP basis sets for all atoms.

General remarks: All chemicals were purchased from Sigma Aldrich or ACROS and were of reagent grade. The chemicals were used without further purification unless stated otherwise. $(n\mathrm{Bu_4N})_2[\mathrm{Mo_6O_{19}}]$[S1] $(n\mathrm{Bu_4N})_4[\alpha\text{-}\mathrm{Mo_8O_{26}}]$,[S1] and $(n\mathrm{Bu_4N})_4[\mathrm{V_4O_{12}}]$[S2] were prepared according to literature references.

2. Synthetic section:

Synthesis of $(n\mathrm{Bu_4N})_3[\mathrm{VMo_5O_{19}}]$:

The synthesis of $(n\mathrm{Bu_4N})_3[\mathrm{VMo_5O_{19}}]$ is a modification of the original synthesis reported by Klemperer *et al*:[S3] $(n\mathrm{Bu_4N})_4[\alpha\text{-}\mathrm{Mo_8O_{26}}]$ (0.242 g, 112 µmol) and $(n\mathrm{Bu_4N})_4[\mathrm{V_4O_{12}}]$ (0.677 g, 496 µmol) are suspended in a N,N-dimethylformamide-water mixture (10 ml, 20:1, v:v). After heating to 80 ℃, the solid materials dissolved and the solution colour intensified to a deep yellow. At this point, 70 mg (1.3 mmol) ammonium chloride are added and the solution is kept at 80 ˚C for 2 h after which the colour had changed to light yellow and slight precipitation was observed. After centrifugation, the yellow solution was crystallized by diffusion of ethyl acetate, giving orange crystals of single-crystal XRD quality as the only solid product. The crystals were washed with diethyl ether and dried under vacuum. Yield: 90 mg, (57 µmol, 32 % based on Mo).

Elemental analysis for $\mathrm{C_{48}H_{108}N_3VMo_5O_{19}}$ (Mw: 1562.02 g/mol) in wt.-% (calcd.): C 37.02 (36.91), H 7.15 (6.97), N 2.74 (2.69), V 3.15 (3.24), Mo 31.21 (31.16).

Characteristic IR bands (in $\mathrm{cm^{-1}}$): 2959 (m), 2874 (s), 1481 (vs), 1152 (m), 976 (s), 935 (s), 874 (s), 795 (s).

Characteristic UV-Vis signals (in acetonitrile): $\lambda_{max,1}$ = 219 nm, ε= 1.70 x 10^4 $\mathrm{M^{-1}\ cm^{-1}}$; $\lambda_{max,2}$ = 265 nm, ε= 1.41 x 10^4 $\mathrm{M^{-1}\ cm^{-1}}$; $\lambda_{max,3}$ = 332 nm, ε= 0.66 x 10^4 $\mathrm{M^{-1}\ cm^{-1}}$; $\lambda_{max,4}$ = 425 nm, ε= 1.12 x 10^3 $\mathrm{M^{-1}\ cm^{-1}}$ (shoulder).

3. Crystallographic information

Single-Crystal Structure Determination: Suitable single crystals of the respective compound were grown and mounted onto the end of a thin glass fiber using Fomblin oil. X-ray diffraction intensity data were measured at 150 K on a Nonius Kappa CCD diffractometer [λ(Mo-K_α) = 0.71073 Å] equipped with a graphite monochromator. Structure solution and refinement was carried out using the SHELX-97 package[S4] *via* WinGX.[S5] Corrections for incident and diffracted beam absorption effects were applied using empirical[S6] or numerical methods.[S7] Structures were solved by a combination of direct methods and difference Fourier syntheses and refined against F^2 by the full-matrix least-squares technique. Crystal data, data collection parameters and refinement statistics are listed in Table S1. These data can be obtained free of charge via www.ccdc.cam.ac.uk/conts/retrieving.html or from the Cambridge Crystallographic Data Center, 12, Union Road, Cambridge CB2 1EZ; fax:(+44) 1223-336-033; or deposit@ccdc.cam.ac.uk. CCDC reference number 831885 (**{VMo$_5$}**).

Table S1: Summary of the crystallographic information for **1**

	Compound **1**
Formula	$C_{48}H_{108}Mo_5N_3O_{19}V_1$
M_r g mol^{-1}	1561.1
crystal	Monoclinic
space	*C*2/c
a [Å]	29.289(2)
b [Å]	18.5771(11)
c [Å]	27.2048(15)
α [º]	90
β [º]	113.438(6)
γ [º]	90
ρ_{cald} [g cm^{-3}]	1.528
V [Å^3]	13580.9(16)
Z	8
μ(Mo$_{K\alpha}$) mm^{-1}	1.090
T [K]	150(2)
no. rflns (measd)	93444
no. rflns (unique)	13854
no. params	706
*R*1 (I>2σ(I))	0.0347
*wR*2 (all data)	0.0993
GooF	1.088

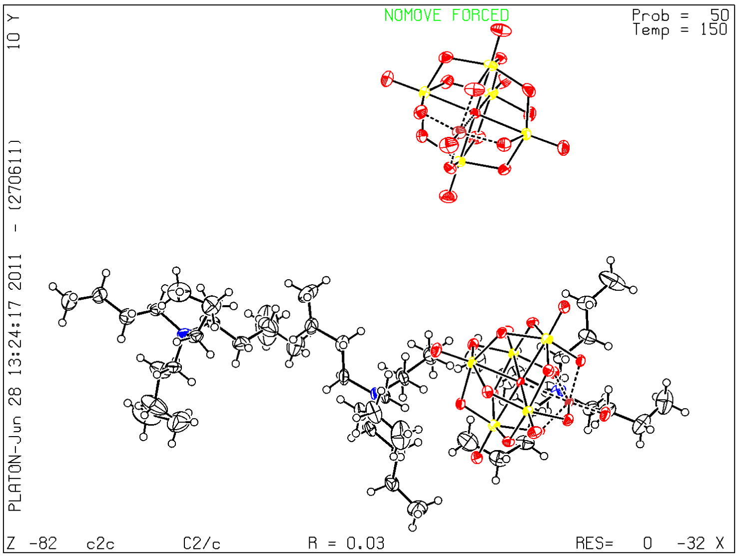

Figure S 1: ORTEP representation of compound **1**, thermal ellipsoids given at 50 % probability. All non-hydrogen atoms were refined anisotropically. Hydrogen atoms were added to the carbon atoms using HFIX and AFIX commands and refined using a riding model.

4. Electrospray ionization mass spectrometry (ESI-MS)

ESI-MS measurements were performed on $(n\mathrm{Bu_4N})_3[\mathrm{VMo_5O_{19}}]$ ([**{VMo$_5$}**] *ca*. 5 x 10^{-5} M in acetonitrile) in negative (-ve) ion mode. Data analysis showed that the base peaks and several other high-intensity peaks were associated with the $[\mathrm{VMo_5O_{19}}]^{3-}$ ion. No other cluster ions were observed. Peak assignments are given in Table S2, see below.

Table S2: Negative mode ESI-MS assignments:

m/z	calculated m/z	Assigned species	Charge	Notes
223.82	223.84	$\{\mathrm{Mo_3O_{10}}\}^{2-}$	2-	fragment
304.68	304.69	$\{\mathrm{HMo_2O_7}\}^{-}$	1-	fragment
386.69	386.72	$\{\mathrm{VMo_2O_9}\}^{-}$	1-	fragment
417.67	417.70	$\{\mathrm{HVMo_5O_{19}}\}^{-}$	1-	
448.67	448.68	$\{\mathrm{HMo_3O_{10}}\}^{-}$	1-	fragment
530.62	530.61	$\{\mathrm{VMo_3O_{12}}\}^{-}$	1-	fragment
689.94	689.96	$\{(n\mathrm{Bu_4N})[\mathrm{Mo_3O_{10}}]\}^{-}$	1-	fragment
1077.66	1077.68	$\{(n\mathrm{Bu_4N})\mathrm{H}[\mathrm{VMo_5O_{19}}]\}^{-}$	1-	base peak
1198.81	1198.82	$\{(n\mathrm{Bu_4N})_3\mathrm{H}[\mathrm{VMo_5O_{19}}]_2\}^{2-}$	2-	Dimer
1318.95	1318.96	$\{(n\mathrm{Bu_4N})_2[\mathrm{VMo_5O_{19}}]\}^{-}$	1-	

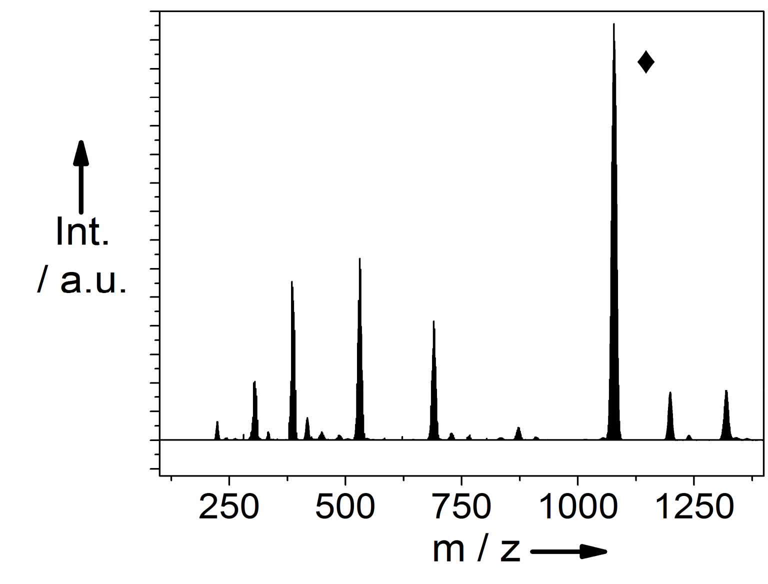

Figure S 2: Negative-mode ESI-mass spectrum for a solution of **1**, $(nBu_4N)_3[VMo_5O_{19}]$ in acetonitrile ([**1**] *ca.* 5 x 10^{-5} M). The base peak (♦) at m/z = 1077.66 corresponds to $\{(nBu_4N)H[VMo_5O_{19}]\}^-$, for further details see Table S2.

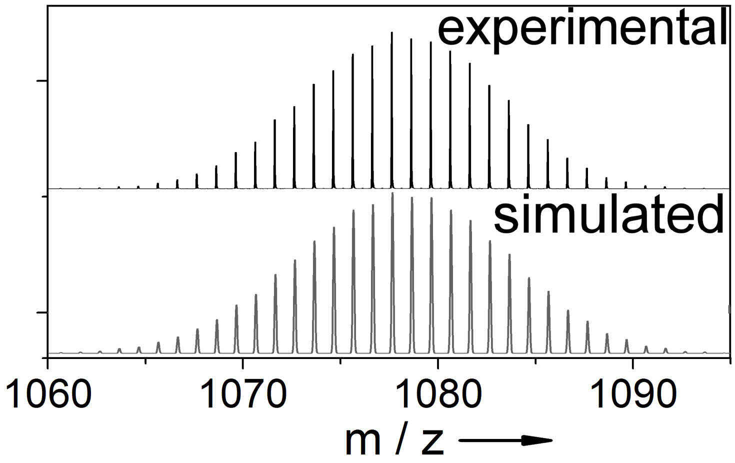

Figure S 3: Negative-mode ESI-mass spectrum for a solution of **1**, showing the experimental and simulated pattern for the base peak at 1077.66, assigned as $\{(nBu_4N)H[VMo_5O_{19}]\}^-$.

5. TD-DFT theoretical calculations

The program package ORCA 2.7 revision 0 was used for all calculations.[S8] The geometries of metal clusters were fully optimized by the spin-restricted DFT method with the BP86 functional[S9,S10] including relativistic effects in zero order regular approximation (ZORA). [S11] The single point calculations were performed with the B3LYP functional[S12,S13] including relativistic effects in zero order regular approximation (ZORA). [S11] For all calculations the triple-ζ basis sets with one-set of polarization functions (TZV(P)) [S14] were used for all atoms. Conductor like screening model (COSMO) was routinely used for all calculations. [S15] TD-DFT calculations were performed using the B3LYP functional and the COSMO with acetonitrile as a solvent. The first 100 excited states were calculated, where the maximum dimension of the expansion space in the Davidson procedure (MAXDIM) was set to 1000. Molecular orbitals were visualized via the program Molekel.[S16]

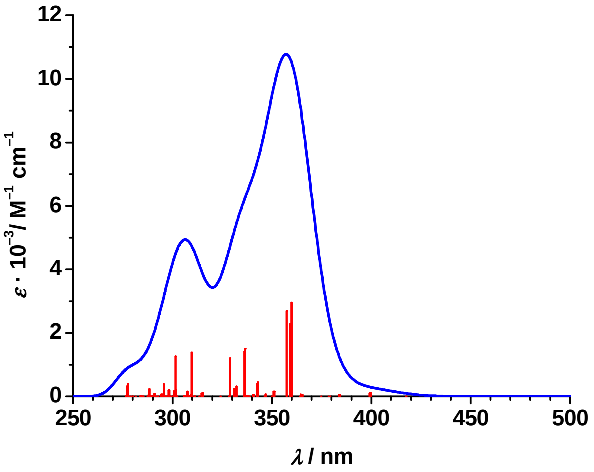

Figure S 4 Electronic absorption spectrum of **{VMo$_5$}** obtained from the spin-restricted B3LYP-ZORA-TD-DFT calculations including the conductor like screening model (COSMO) with acetonitrile as a solvent. The first 100 excited states have been calculated. Full-width at half-maximum (FWHM) height was set to 2000 cm^{-1} for each transition.

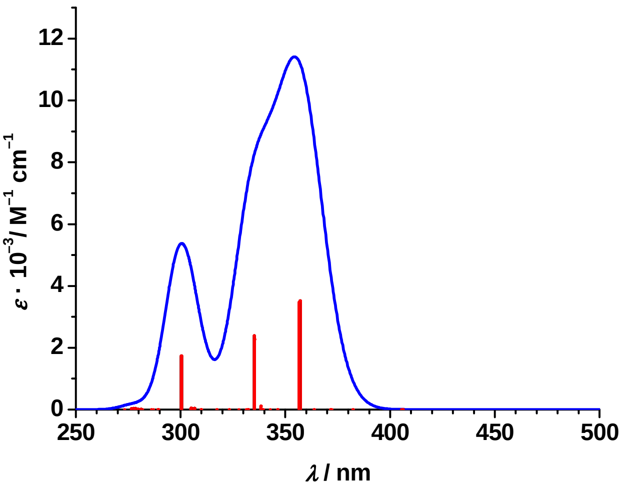

Figure S 5: Electronic absorption spectrum of **{Mo$_6$}** obtained from the spin-restricted B3LYP-ZORA-TD-DFT calculations including the conductor like screening model (COSMO) with acetonitrile as a solvent. The first 100 excited states have been calculated. Full-width at half-maximum (FWHM) height was set to 2000 cm^{-1} for each transition.

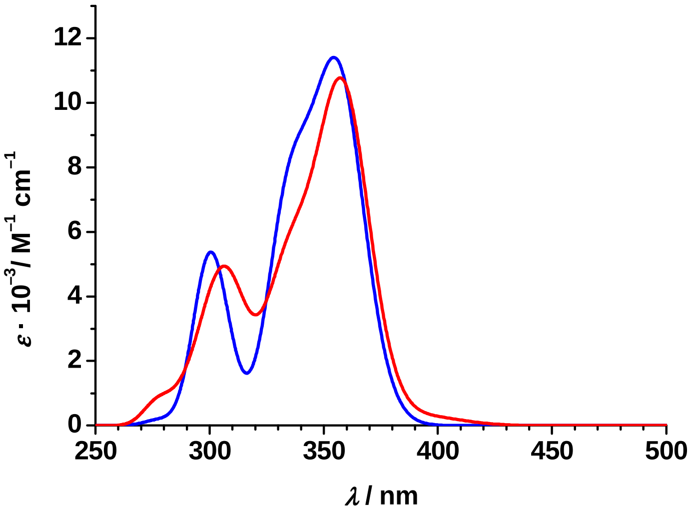

Figure S 6: Superimposed electronic absorption spectra of **{Mo$_6$}** (in blue) and **{VMo$_5$}** (in red) obtained from the spin-restricted B3LYP-ZORA-TD-DFT calculations including the conductor like screening model (COSMO) with acetonitrile as a solvent. The first 100 excited states have been calculated for both metal clusters. Full-width at half-maximum (FWHM) height was set to 2000 cm^{-1} for each transition.

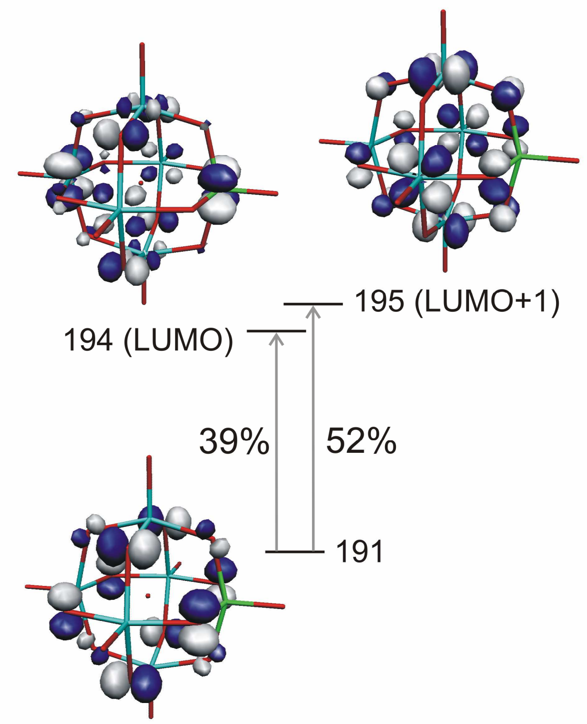

Figure S 7: The leading configurations present in the excited state 2 (399.8 nm) of **{VMo$_5$}**. The Kohn-Sham orbitals obtained from the spin-restricted B3LYP-ZORA-TD-DFT calculations including the conductor like screening model (COSMO) with acetonitrile as a solvent are shown.

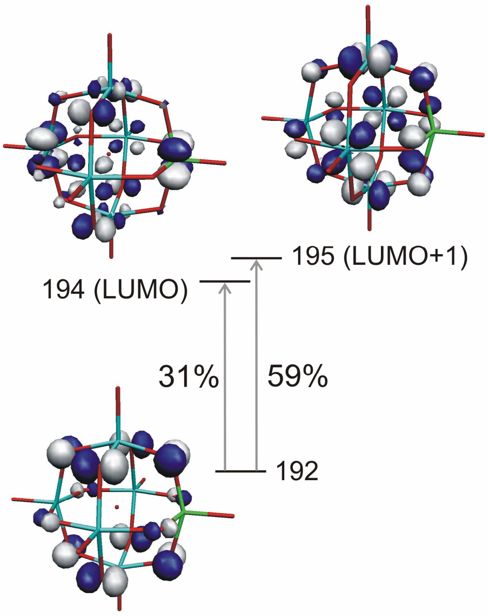

Figure S 8: The leading configurations present in the excited state 3 (399.2 nm) of **{VMo$_5$}**. The Kohn-Sham orbitals obtained from the spin-restricted B3LYP-ZORA-TD-DFT calculations including the conductor like screening model (COSMO) with acetonitrile as a solvent are shown.

Table S3. The first 20 excited states for **{VMo$_5$}** obtained from the spin-restricted B3LYP-ZORA-TD-DFT calculations including the conductor like screening model (COSMO) with acetonitrile as a solvent.

state	energy, cm^{-1}	wavelength, nm	oscillator strength	O→V character, %
1	23946	417.6	0.000003	–[a]
2	25010	399.8	0.000970	10
3	25052	399.2	0.000905	8
4	26019	384.3	0.000403	–
5	26050	383.9	0.000504	–
6	26361	379.3	0.000005	–
7	26417	378.5	0.000000	–
8	26677	374.9	0.000001	–
9	27375	365.3	0.000493	–
10	27431	364.6	0.000580	–
11	27459	364.2	0.000001	–
12	27793	359.8	0.010522	5
13	27788	359.9	0.027279	12
14	27833	359.3	0.021001	7
15	27839	359.2	0.005092	–
16	27981	357.4	0.024821	–
17	28463	351.3	0.001376	–
18	28485	351.1	0.001279	–
19	28573	350.0	0.000018	–
20	28496	350.9	0.001445	–

[a] Less than 1%, exact value is not determined.

Table S4. Composition of the low-energy states for **{VMo$_5$}** with significant O→V LMCT character obtained from the spin-restricted B3LYP-ZORA-TD-DFT calculations including the conductor like screening model (COSMO) with acetonitrile as a solvent.

state	excitation	excitation weight, %	assignment	O→V character, %
2	191 → 194	39	O→Mo / π→π*[a] / O→V	26
	191 → 195	52	O→Mo / π→π*	0
3	192 → 194	31	O→Mo / π→π* / O→V	26
	192 → 195	59	O→Mo / π→π*	0
12	189 → 195	55	O→Mo / π→π*	0
	191 → 194	18	O→Mo / π→π* / O→V	26
	191 → 195	12	O→Mo / π→π*	0
13	188 → 195	16	O→Mo / π→π*	0
	192 → 194	45	O→Mo / π→π* / O→V	26
	192 → 195	23	O→Mo / π→π*	0
14	189 → 195	19	O→Mo / π→π*	0
	191 → 194	26	O→Mo / π→π* / O→V	26
	191 → 195	21	O→Mo / π→π*	0
	193 → 196	21	O→Mo / π→π*	0

[a] Transition between oxygen-centered molecular orbitals.

Table S5. Composition of the donor and acceptor orbitals involved in low-energy electronic transitions for **{VMo$_5$}** obtained from the spin-restricted B3LYP-ZORA-DFT calculations including the conductor like screening model (COSMO) with acetonitrile as a solvent.

MO	occupation	Mo, %	O, %	V, %
185	2	3.2	96.6	0.2
186	2	2.8	96.4	0.8
187	2	2.8	96.4	0.8
188	2	3.2	96.7	0.1
189	2	3.1	96.7	0.1
190	2	2.8	96.5	0.7
191	2	0.4	99.5	0.1
192	2	0.4	99.5	0.1
193	2	0.5	99.5	0.0
194	0	41.1	32.4	26.6
195	0	60.3	39.6	0.0
196	0	70.4	28.7	1.0
197	0	70.7	28.6	0.7
198	0	38.8	23.3	38.0
199	0	68.1	31.9	0.0
200	0	53.3	31.5	15.3

Table S6. Coordinates of **{VMo_5}** optimized with the spin-restricted BP-ZORA-DFT including the conductor like screening model (COSMO) with acetonitrile as a solvent.

Mo	8.538588	5.046749	2.434425
Mo	7.098769	2.706437	4.316186
Mo	8.951733	5.043993	5.733992
Mo	7.097969	7.382681	4.316801
O	7.144137	5.045457	4.257830
O	9.591713	5.044403	1.059691
O	8.267786	3.151433	2.794210
O	9.769710	5.045479	3.943260
O	8.268937	6.939934	2.792991
O	7.101418	0.977497	4.312605
O	5.618055	3.142630	3.122827
O	10.327209	5.045635	6.780771
O	8.632407	6.946387	5.438287
O	7.101413	9.111626	4.312522
O	6.765433	5.045693	1.641628
V	5.721314	5.046651	6.122863
O	4.740531	5.043632	7.406017
O	5.979310	3.187088	5.776012
Mo	5.244808	5.043685	2.900700
O	4.505547	5.045046	4.650172
O	5.977514	6.903596	5.778283
O	8.633769	3.143053	5.438584
O	7.452529	5.044810	6.908071
O	5.618768	6.946783	3.124048
O	3.875797	5.045409	1.845208

Table S7. Coordinates of **{Mo_6}** optimized with the spin-restricted BP-ZORA-DFT including the conductor like screening model (COSMO) with acetonitrile as a solvent.

Mo	8.549891	5.046987	2.423516
Mo	7.121007	2.692493	4.288316
Mo	8.985495	5.043133	5.717078
Mo	7.121007	7.397877	4.288313
O	7.121008	5.045162	4.288315
O	9.591822	5.045768	1.060334
O	8.269541	3.153758	2.788012
O	9.771881	5.044690	3.936060
O	8.271027	6.937884	2.786201
O	7.121007	0.976021	4.288343
O	5.618667	3.152455	3.138329
O	10.349652	5.044279	6.757748
O	8.621248	6.936464	5.436793
O	7.121005	9.114151	4.288302
O	6.769057	5.044629	1.637150
Mo	5.692131	5.046993	6.153124
O	4.650205	5.045765	7.516310
O	5.972476	3.153762	5.788610
Mo	5.256519	5.043128	2.859561
O	4.470138	5.044687	4.640572
O	5.970986	6.937873	5.790435
O	8.623345	3.152451	5.438289
O	7.472961	5.044613	6.939489
O	5.620762	6.936475	3.139861
O	3.892357	5.044286	1.818895

6. UV-Vis spectroscopic investigations

Photocatalytic studies of the decomposition of patent blue V (= PBV) were typically performed at cluster concentrations of 5.0 μM and dye concentrations of 20 μM in acetonitrile:water mixtures (4:1, v:v) unless stated otherwise. The samples were irradiated using a 150 W medium-pressure mercury light source (Heraeus TQ-150, UV-Consulting Peschl) equipped with a pyrex deep-UV cutoff filter λ_{cutoff} = 320 nm. For visible-light irradiation, a custom-built P = 3 W LED light source (λ_{max} = 470 nm) was used. Samples were irradiated under stirring and samples were taken at timed intervals und analyzed using UV-Vis spectrophotometry.

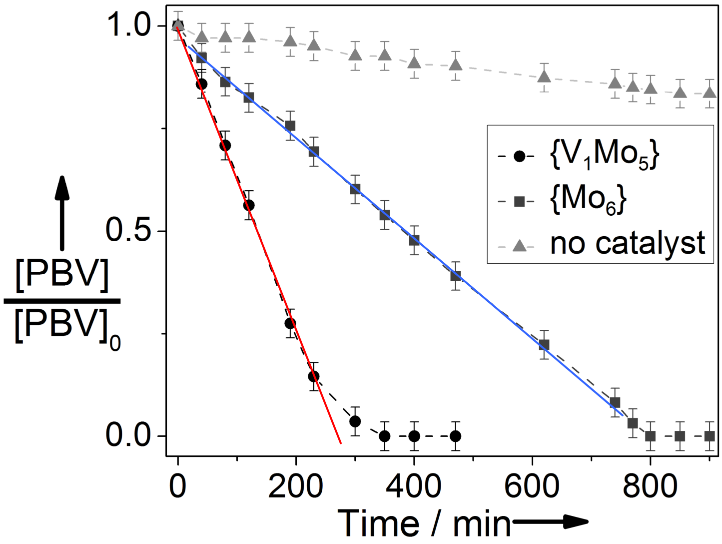

Figure S 9: Comparative UV-light induced PBV decomposition, showing faster PBV decomposition by **{VMo$_5$}** (•) as compared with **{Mo$_6$}** (■). Conditions: Pure PBV (▲) was used as a reference. Conditions: medium-pressure mercury light source, P = 150 W; solvent: acetonitrile:water (4:1, v:v); [PBV]$_0$ =20 μM; [**{VMo$_5$}**] = [**{Mo$_6$}**] = 5.0 μM. PBV = patent blue V. Red and blue lines indicate the linear fits for rate constant determination.

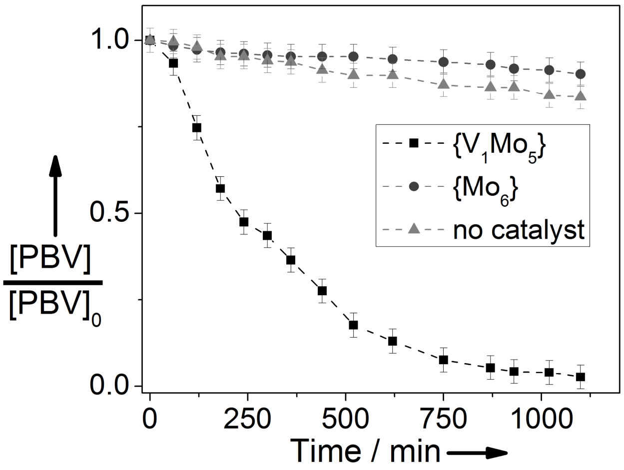

Figure S 10: Comparative visible-light induced PBV decomposition. For **{VMo$_5$}**, photooxidative activity can still be observed (■); **{Mo$_6$}** does not show any photocatalytic activity (•). Conditions: Pure PBV (▲) was used as a reference. Conditions: LED-irradiation, λ_{max} = 470 nm, P = 3 W; solvent: acetonitrile:water (4:1, v:v); [PBV]$_0$ =25.7 μM; [**{VMo$_5$}**] = [**{Mo$_6$}**] = 1.25 mM. PBV = patent blue V.

Time-dependent spectral investigation of PBV decomposition

To follow the PBV decomposition spectroscopically, the reaction was monitored at timed intervals in order to establish the formation of any reduced cluster species. However, no significant amount of reduced cluster species (expected absorption around 600-800 nm) was observed, see Fig. S11.

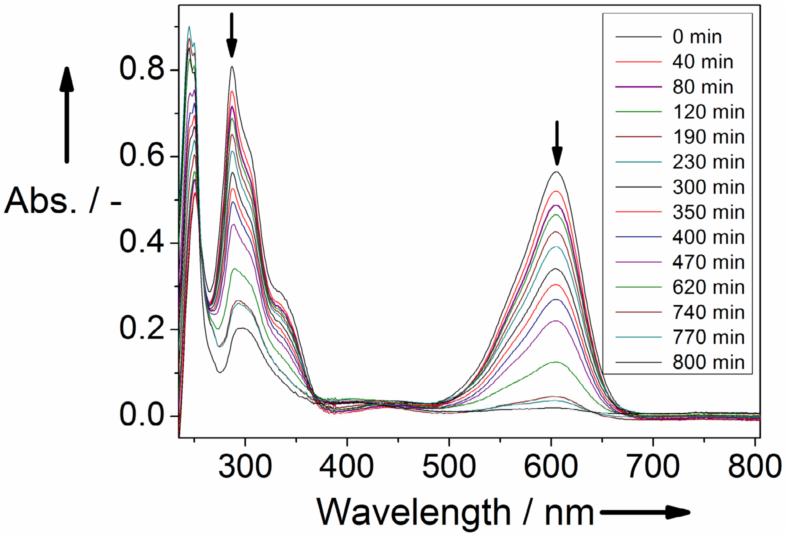

Figure S 11: Time-dependent UV-Vis spectroscopic monitoring of the PBV decomposition. Peaks attributed to the PBV dye were observed to decrease with time

.

Determination of the turnover number TON and turnover frequency TOF

Turnover number and turnover frequency were determined under the following reaction conditions: $[PBV]_0$ = 164 µM; [**{VMo$_5$}**] = [**{Mo$_6$}**] = 0.10 µM. irradiation source: 150 W medium pressure UV light source with cutoff filter (λ_{cutoff} = 320 nm); solvent: acetonitrile:water (4:1, v:v). Dye decomposition was followed UV-Vis spectroscopically until no further PBV decomposition was detected. From the initial and final PBV concentrations, turnover numbers and turnover frequencies were determined: For **{VMo$_5$}**, $TON_{\{\mathrm{VMo5}\}}$ = 1606 and $TOF_{\{\mathrm{VMo5}\}}$ = 5.35 min^{-1} were found, for **{Mo$_6$}**, $TON_{\{\mathrm{Mo6}\}}$ = 1308 and $TOF_{\{\mathrm{Mo6}\}}$ = 1.92 min^{-1} were found.

7. Cyclic Voltammetry

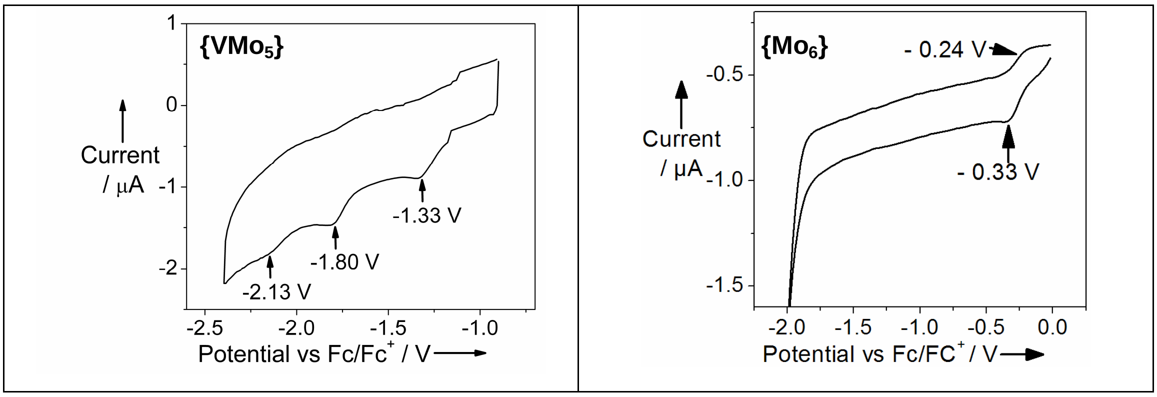

Figure S 12: Left: Cyclovoltammogram of $(n\mathrm{Bu}_4\mathrm{N})_3[\mathrm{VMo}_5\mathrm{O}_{19}]$ showing three irreversible reduction peaks at -1.33 V, -1.80 V and -2.13 V. Based on typical vanadium vs molybdenum reduction potentials, the peak at -1.33 V can be assigned to the $V^{5+/4+}$ reduction, the peaks at -1.80 V and -2.13 V can be assigned to $Mo^{6+/5+}$ reductions. Right: Cyclovoltammogram of $(n\mathrm{Bu}_4\mathrm{N})_2[\mathrm{Mo}_6\mathrm{O}_{19}]$, showing one reversible redox-event centered at -0.29 which is assigned to the $Mo^{6+/5+}$ redox-couple. Conditions: solvent: dried acetonitrile, [**{VMo$_5$}/{Mo$_6$}**] *ca.* 1 mM. Electrolyte: $TBAPF_6$, 0.1 M), scan rate: 50 mV/s.

8. Literature references cited in Supporting Information

[S1] N. H. Hur, W. G. Klemperer, R.-C. Wang, *Inorg. Synth.* **1990**, *27*, 77.

[S2] J. Forster, B. Rösner, M. M. Khusniyarov, C. Streb, *Chem. Commun.* **2011**, *47*, 3114

[S3] M. Filowitz, R. K. C. Ho, W. G. Klemperer, W. Shum, *Inorg. Chem.* **1979**, *18*, 93-103

[S4] G. M. Sheldrick, *Acta Crystallogr.* 2008, **A64**, 112.

[S5] L. J. Farrugia, *J. Appl. Cryst.* 1999, **32**, 837.

[S6] R. H. Blessing, *Acta Crystallogr. A* 1995, **51**, 33.

[S7] P. Coppens, L. Leiserowitz, D. Rabinovich, *Acta Crystallogr.* 1965, **18**, 1035.

[S8] F. Neese, *ORCA – an Ab Initio, Density Functional and Semiempirical SCF-MO Package, version 2.7 revision 0;* Institut für Physikalische und Theoretische Chemie, Universität Bonn, Germany, ***2009***.

[S9] A. D. Becke, *Phys. Rev. A* **1988**, *38*, 3098.

[S10] J. P. Perdew, *Phys. Rev. B* **1986**, *34*, 7406.

[S11] C. van Wüllen, *J. Chem. Phys.* **1998**, *109*, 392.

[S12] A. D. Becke, *J. Chem. Phys.* **1993**, *98*, 5648.

[S13] C. T. Lee, W. T. Yang, R. G. Parr, *Phys. Rev. B* **1988**, *37*, 785.

[S14] D. A. Pantazis, X. Y. Chen, C. R. Landis, F. Neese, *J. Chem. Theory Comput.* **2008**, *4*, 908.

[S15] A. Klamt, G. Schüürmann, *J. Chem. Soc., Perkin Trans. 2* **1993**, 799.

[S16] S. Portmann, *Molekel, version 4.3.win32; CSCS/UNI Geneva, Switzerland,* **2002**.